Struct Multidisc Optim (2016) 53:321–338
DOI 10.1007/s00158-015-1315-z

INDUSTRIAL APPLICATION

Crashworthiness design of vehicle structure with tailor rolled blank

Libin Duan[1,2] · **Guangyong Sun**[1,2] · **Junjia Cui**[1,2] · **Tao Chen**[1,2] · **Aiguo Cheng**[1,2] · **Guangyao Li**[1,2]

Received: 25 November 2014 / Revised: 10 August 2015 / Accepted: 22 August 2015 / Published online: 30 September 2015
© Springer-Verlag Berlin Heidelberg 2015

Abstract Lightweight and crashworthiness design have been two main challenges in the vehicle industry. These two performances often conflict with each other. To not sacrifice vehicle crashworthiness performance when performing vehicle lightweight design, a novel inner part of front longitudinal beam (FLB-inner) structure with a tailor rolled blank (TRB) concept is proposed in this work, and the corresponding design method is also proposed to minimize the weight of FLB-inner. Firstly, a full-scale vehicle finite element model is adopted and experimentally verified. Secondly, the conventional uniform thickness FLB-inner panel is replaced with a TRB structure, herein, the FLB-inner is divided into four segments with different thickness according to the crashworthiness requirements of frontal impact. Then the material constitutive model and finite element modeling for TRB is established. Thirdly, the optimal Latin hypercube sampling (OLHS) technique is used to generate sampling points and the objective and constraints function values are calculated using commercial software LS-DYNA. Based on the simulation results, the ε-SVR surrogate models are constructed. Finally, the artificial bee colony (ABC) algorithm is applied to obtain the optimal thickness distribution of FLB-inner. The results indicated that the weight of the FLB-inner is reduced by 15.21 %, while the crashworthiness is mproved in comparison with the baseline design.

Keywords Tailor rolled blank (TRB) · Front longitudinal beam (FLB) · Lightweight design · Crashworthiness optimization · Artificial bee colony (ABC)

Nomenclature

TRB	Tailor rolled blank
TWB	Tailor welded blank
CTZ	Constant thickness zone
TTZ	Thickness transition zone
FLB	Front longitudinal beam
CLB	Center longitudinal beam
FLB-inner	Inner part of the front longitudinal beam
FLB-TRB	Front longitudinal beam with TRB
TRB FLB-inner	Inner part of front longitudinal beam with TRB
EA	Energy absorption
UHSS	Ultra high strength steel
AHSS	Advanced high strength steel
OLHS	Optimal Latin hypercube sampling
ABC	Artificial bee colony
FSV	Future Steel Vehicle
MDO	Multidisciplinary design optimization
BIW	Body-in-white
RSM	Response surface models
RBF	Radial basis functions
MARS	Multivariate adaptive regression splines
KG	Kriging
SVR	Support vector regression
ε-SVR	ε-support vector regression
ν-SVR	ν-support vector regression

✉ Aiguo Cheng
cheng_aiguo@163.com

✉ Guangyao Li
gyli@hnu.edu.cn

[1] State Key Laboratory of Advanced Design and Manufacturing for Vehicle Body, Hunan University, Changsha 410082, China

[2] Collaborative Innovation Center of Intelligent New Energy Vehicle, Shanghai 200092, China

1 Introduction

Recently, energy consumption and emissions, environment protection and vehicle safety have been main challenges in vehicle industry. It is reported that a saving of 100 kg of vehicle weight allows for a reduction of fuel consumption of about 0.35 l/100 km and CO_2 emissions saving of 8.4 g/km (Goede et al. 2009). As body-in-white (BIW) weighs about 25 % of the whole vehicle, lightweight design of BIW plays a significant role in decreasing the weight of full vehicles. Furthermore, due to stricter safety regulations and environmental pressures, vehicle crashworthiness and lightweight should be taken into consideration simultaneously. The traditional lightweight method is to use high strength steel (HSS) or ultra-high strength steel (UHSS). In this regards, the future steel vehicle (FSV-Final Engineering Report 2011) reduced mass by more than 39 % over a benchmark vehicle by using HSS and UHSS. Li et al. (2003) and Zhang et al. (2006) adopted HSS to reduce the weight of vehicle structures. However, the high prices of these materials hinder the large-scale application in BIW parts. In addition, the conventional uniform thickness structures mainly use single material and uniform wall thickness. In fact, automotive components often bear very complex loading, which implies that different regions should have different roles to maximize usage of materials. Obviously, potential of crashworthiness and lightweight of the conventional uniform thickness structures has not been fully exploited. In order to address the issue, some advanced manufacturing processes, such as tailor welded blank (TWB) and tailor rolled blank (TRB) have been presented and widely applied in automotive industry. In the application of TWB, the inner door panel (Li et al. 2015a), B-pillar (Pan et al. 2010) and frontal side rail (Shi et al. 2007) are some typical examples.

Compared with TWB, TRB varies the blank thickness with a continuous thickness transition through adjusting the roll gap (see Fig. 1), which leads to have better formability and greater weight reduction (Meyer et al. 2008). The advantages of TRB are as follows (Kopp et al. 2005b): (1) production costs of TRBs do not depend on the number of thickness transitions; (2) any thickness transition can be chosen within the process limits, see Fig. 1; (3) there are no stress peaks across the transition due to the smooth thickness transitions; (4) TRBs have good forming characteristics because of the elimination of welding seams and corresponding heat-affected zones in TRBs. Due to the advantage of TRB, numerous studies have been conducted. In this regards, the company Mubea mastered the key manufacturing technology for TRB and had the capability of producing 70,000 t TRB with the maximum sheet width up to 750 mm per year (Muhr und Bender KG 2013). The institute of metal forming (IBF) performed deep drawing tests of TRB using experimental and numerical methods (Kopp et al. 2005a). Meyer et al. (2008) also investigated the deep drawing behaviors of TRB numerically and experimentally. Ryabkov et al. (2008) presented a novel manufacturing process for TRB whose thickness can continuously vary in longitudinal and lateral direction through 3D-strip profile rolling. Zhang et al. (2012a, b) investigated the springback characteristics of U-channel with TRB. Beiter and Groche (2011) focused on the development of novel lightweight profiles for automotive industries by roll forming of tailor rolled blanks. Jeon et al. (2011) developed a vehicle door inner panel using TRB. Sun and his co-authors (Sun et al. 2014; Li et al. 2015a, b) studied the crashworthiness of TRB thin-walled structures under axial impact, and further compared the energy absorption characteristic between TRB columns and tapered tubes withstanding oblique impact load. Lately, Sun et al. (2015) first investigated the crashworthiness of TRB tubes under dynamic bending load. Though the TRB structures have excellent crashworthiness, it is not easy to obtain the optimal thickness distribution. As an effective alternative, the structural optimization methodology is used to design the TRB parts. For example, Chuang et al. (2008) adopted a multidisciplinary design optimization methodology to obtain the optimal thickness profiles of underbody parts.

It is well known that front longitudinal beam (FLB) is the most significant deformable part under vehicle frontal impact and its deformation pattern can greatly influence the vehicle safety (Gu et al. 2013). To the authors' best knowledge, there have been very limited reports available on the crashworthiness design of front longitudinal beam with TRB (FLB-TRB). Therefore, the paper aims to performing the lightweight design of the FLB-TRB under crashworthiness criteria. In the whole design process, the initial FLB-inner is first presented according to the crashworthiness requirements of frontal impact. Then the material constitutive model and finite element modeling for TRB is established. Following this, the optimization technique, in which the optimal Latin hypercube sampling (OLHS) technique, ε-SVR surrogate models and artificial bee colony (ABC) algorithm are integrated, is presented to obtain the optimal thickness distribution of FLB-inner. The results indicated that the TRB structures have excellent potential for crashworthiness and lightweight.

2 Problem descriptions

2.1 Basic principles of frontal impact crashworthiness design

The main means of improving vehicle safety under full width frontal impact is to reduce the peak acceleration

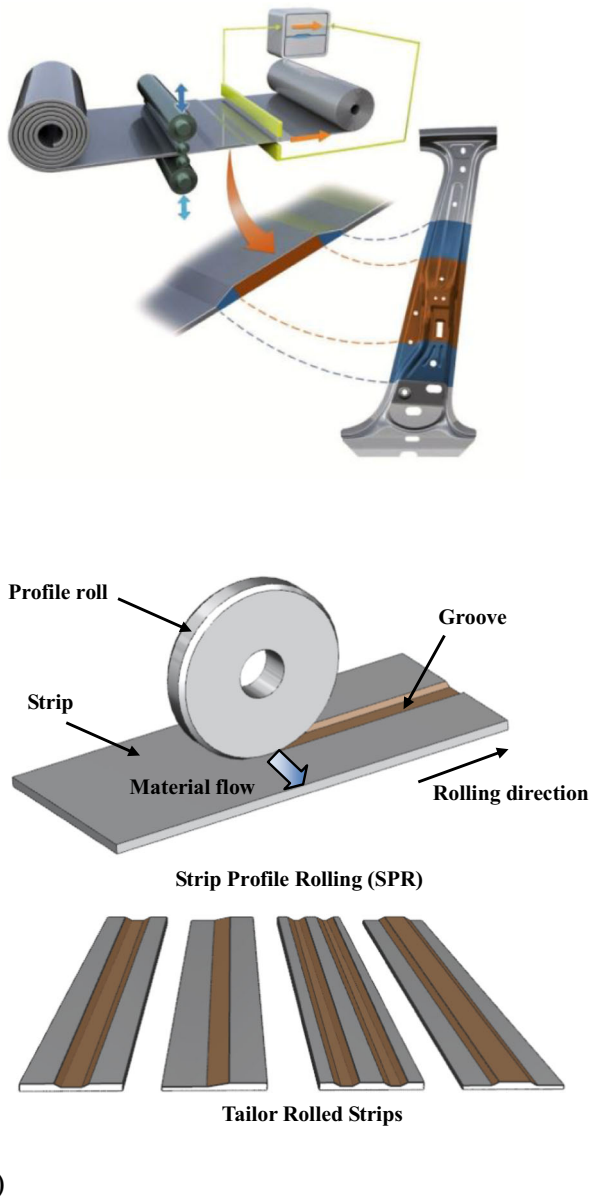

Fig. 1 Two rolling processes for producing flexibly rolled blanks (**a**) Flexible rolling process for longitudinal thickness transitions (Kopp et al. 2005b) (**b**) Strip profile rolling process for latitudinal thickness transitions (Hirt and Dávalos-Julca 2012)

and minimize the dash panel intrusion. Generally, vehicle front end can be divided into three classic function zones: safety cage, transition zone and crush zone, as shown in Fig. 2. The safety cage is used to resist crash load and maintain the integrity of passenger compartment. The main role of the transition zone is to transfer he crash loads from front end to the back end of vehicle, while the main role of the crush zone is to absorb as much as possible the kinetic energy by plastic deformation modes.

Figure 3 shows the transmission path of crash load under frontal impact. The energy absorption (EA) and EA ratio of the key deformable parts are listed in Table 1. It can be seen that the FLB is the main load path, which transfers 70 % of the crash load and absorbs more than 50 % of the EA. From this perspective, the FLB is the most significant part under vehicle frontal impact. In other words, the design quality of FLB will directly determine the vehicle safety to some extent.

As we all known, the FLB has a mixed axial and bending deformation pattern under vehicle frontal impact. Compared with the bending deformation, the axial deformation mode is a preferred pattern to absorb kinetic energy. To fully take advantage of the crush space of crush zone and exploit the maximum energy absorption potential, the FLB is divided into 4 different spaces, as shown in Fig. 4, where ‘space A’ and ‘space B’ are expected to generate a relatively uniform and progressive axial collapse, ‘space C’ is defined by the dimensions of the engine compartment and ‘space D’ expects high bending stiffness to resist bending deformation. Among these spaces, the ‘space A’, ‘space B’ and ‘space C’ belong to the

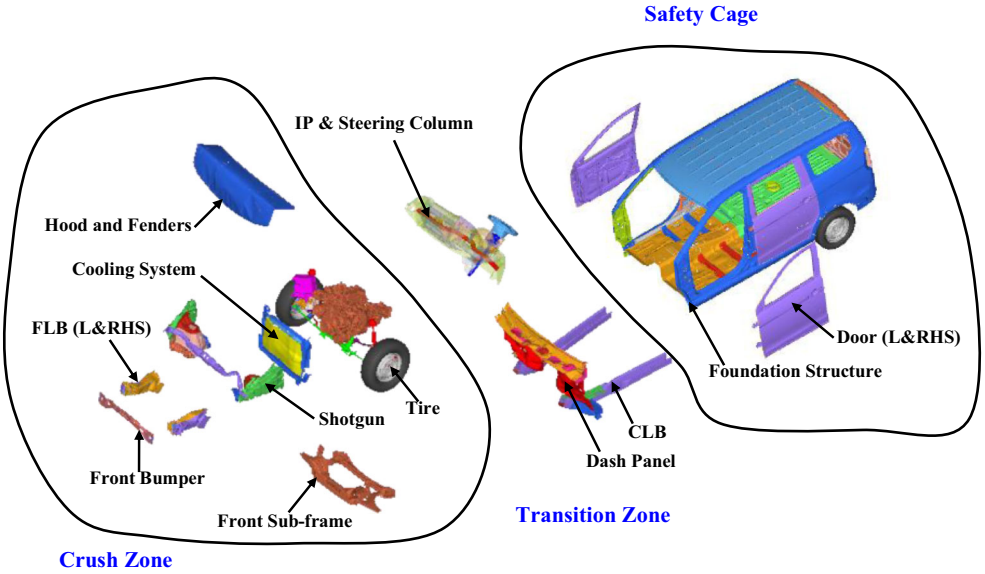

Fig. 2 Design framework for vehicle crashworthiness: classic function zones under frontal impact

crush zone, which are used to absorb kinetic energy, while the 'space D' belongs to the transition zone, whose main aim is to transfer impact load.

In order to satisfy the design requirements of crush space management, the traditional FLB must add some small reinforcements or brackets into it. However, this method will inevitably increase the manufacturing costs and the mass of FLB. Fortunately, the tailor rolled blank (TRB) technique can easily realize the requirements of crush space management of front end structure by adjusting the blank thickness. Therefore, the objective of this work is to maximize its weight reduction without compromising vehicle crashworthiness performances by combining the advantages of TRB manufacturing technique. For simplicity, the FLB-inner is taken as an example to demonstrate the design progress in this study. Of course, the design methodology also serves as a good example for the design of other parts.

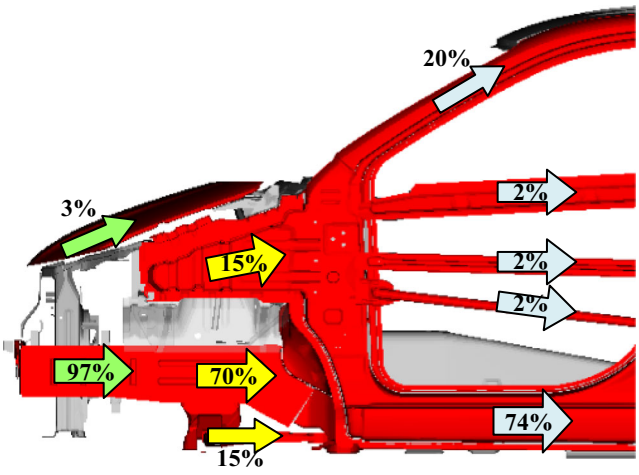

Fig. 3 Load path distribution for frontal impact crash

2.2 Finite element modeling for TRB FLB-inner

Figure 1 shows the schematic diagram of the whole manufacturing process of the TRB, whose customized thickness can continuously vary along the rolling direction by adjusting the roll gap. The different roll spacing will produce different strain hardening, which directly results in different material properties. As a result, the variability of thicknesses and material properties in different local zones has to be considered in the numerical simulation of the TRB FLB-inner. In order to address the issue, effective plastic stress–strain field should be constructed firstly. Then the FE model of the TRB FLB-inner is modeled.

Table 1 EA and EA ratio of the key deformable parts

NO.	Component name		EA (J)	EA Ratio (%)	
1	Front longitudinal beam (FLB) (L&RHS)	Inner	38,471.23	34.13 %	54.11 %
		Outer	12,281.35	10.89 %	
		Reinforcement	10,250.11	9.09 %	
2	Center longitudinal beam (CLB) (L&RHS)		3301.42	2.93 %	
3	Front bumper		4772.76	4.23 %	
4	Dash panel		2951.34	2.62 %	
5	Floor		1303.70	1.16 %	
6	Shotgun (L&RHS)		2288.39	2.03 %	
7	Windscreen cross member		872.61	0.77 %	
8	Cooling system		3025.98	2.68 %	
9	A-pillar lower (L&RHS)		2947.45	2.61 %	
10	Tire (L&RHS)		1187.82	1.05 %	
11	Front sub-frame		4680.28	4.15 %	
12	Transmission system		3041.70	2.70 %	
13	Other		21,353.04	18.94 %	

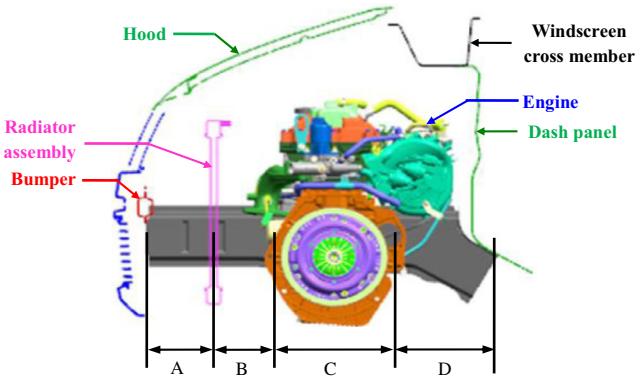

Fig. 4 Crush space management for front end structure

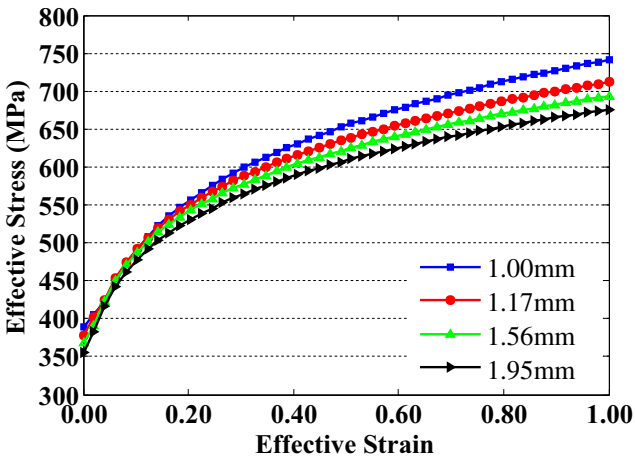

Fig. 6 Effective stress–strain curves of HSLA340 with different thicknesses

2.2.1 Material constitutive model for TRB

The material of the TRB FLB-inner is steel HSLA340 with mechanical properties of density $\rho=7.8\times10^3$ kg/m^3, Young's modulus $E=210$ GPa, Poisson's ratio $v=0.30$. Up to today, there is no material constitutive model for TRB available. In order to establish a relationship of strain vs. stress for TRB made of the steel grade HSLA340, four specimens with thickness of 1.00, 1.17, 1.56 and 1.95 mm, which are taken in the rolling direction, are used to perform uniaxial tensile tests on an INSTRON-5581 electronic universal testing machine, as shown in Fig. 5.

The effective stress vs. effective strain curves derived from test results are given in Fig. 6. From which it is easily found that the material properties of HSLA340 have a significant difference among the different thicknesses. The yield strength of thinner blanks is higher than that of thicker blanks. However, the slope of the thicker blanks is slightly higher than that of thinner blanks until the effective strain is up to 0.2. Due to the expensive cost and time consuming of experimental tests, it is impractical to obtain the material characteristics of

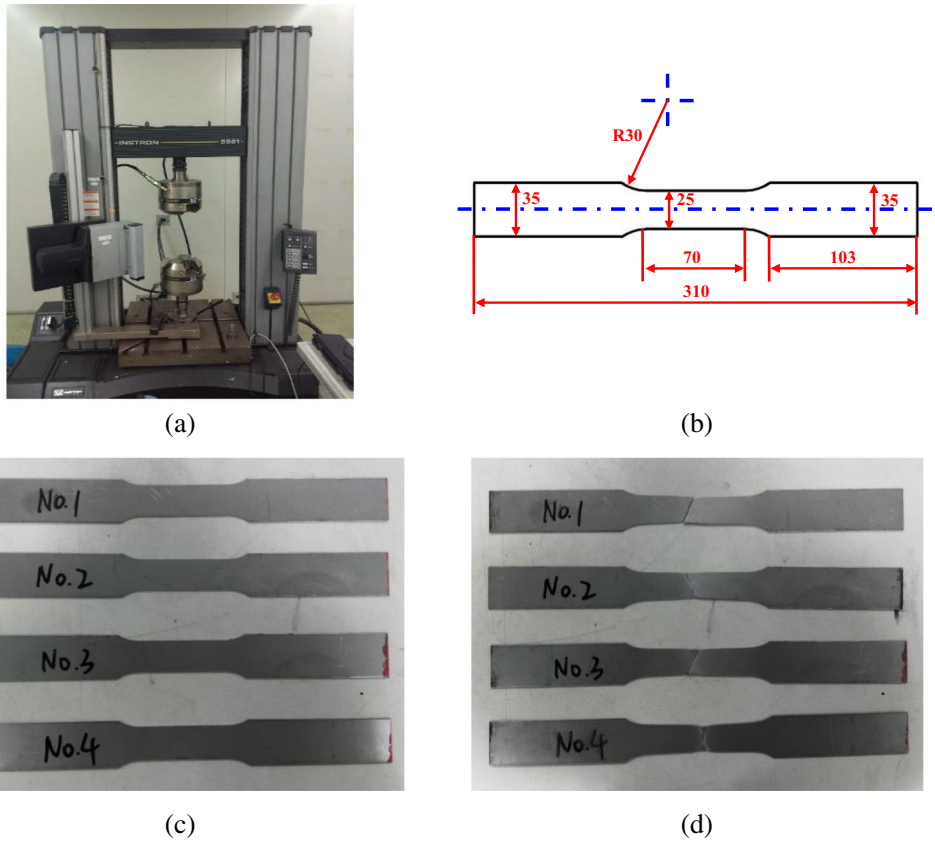

(a) (b)

(c) (d)

Fig. 5 (**a**) INSTRON-5581; (**b**) dimension of the HSLA340 steel specimens with uniaxial tension (unit: mm); (**c**) initial specimens; and (**d**) deformed specimens

any thickness by experimental method. To address the issue, the Lagrange polynomial interpolation method is used to complete the construction of the effective stress vs. effective strain field of TRBs made of high-strength steel grade HSLA340, as shown in Fig. 7.

2.2.2 Finite element modeling

Figure 8a depicts the geometry model of the TRB FLB-inner. To model the variable thickness of TRB, the 8-nodes thick shell element (T-shell in LS-DYNA) (Halquist 2007) was adopted. The schematic diagram of T-shell is shown in Fig. 8b. The element of the constant thickness zone (CTZ), which has uniform mechanical property, is organized as a single component, while the thickness transition zone (TTZ) needs to be divided into several components because it has non-uniform mechanical properties, as shown in Fig. 8b. The number of the components is decided by the modeling accuracy. A higher number leads generally to a higher accuracy. The material model used in the finite element modeling is piecewise linear plasticity material law (Mat 24 in LS-DYNA). The material performance of every component is calculated according to its thickness from Fig. 7. The major contact algorithms used are "automatic single surface" contact that considers self-contact between sheet elements, "automatic surface to surface" and "automatic node to surface". In the simulation, strain rate effects are taken into account in the analysis since HSLA340 belongs to high strength steel, which typically exhibits strain rate dependence. The effect is accounted through the Cowper Symonds model (Halquist 2007) given as:

$$\sigma_y = \sigma_0 \left[1 + \left(\frac{\dot{\varepsilon}}{C} \right)^{\frac{1}{P}} \right] \tag{1}$$

where $\dot{\varepsilon}$ is the strain rate, σ_0 is yield strength, σ_y is the scaled yield strength. C and P are respectively the strain rate parameters.

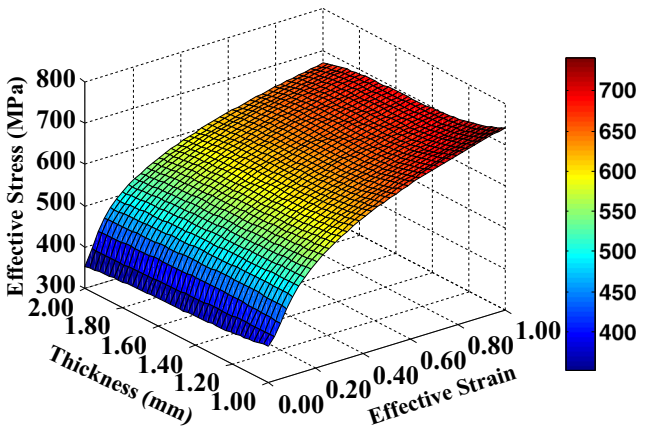

Fig. 7 Effective stress- strain field of TRBs made of steel grade HSLA340

2.3 Finite element modeling for full-scale vehicle

The crashworthiness design will be based on a FE model of full-scale vehicle, which consists of 972,074 shell elements, 502 solid elements, 6063 beam elements, 1, 004,414 nodes and 502 components with 1350 kg. For these shell elements, around 95 % are 4-node Belytschko-Tsay shell elements with average mesh size of 10 mm. Approximately 5×5 mm shell elements are used in the key deformable structures. The hourglass control is employed to avoid the elements with spurious energies caused by reduced integration. Finally, the inertial characteristics of the whole vehicle model are checked against the actual vehicle, in which the concentrated masses are added to ensure the model inertia. It is noted that the structural crashworthiness is performed without considering the detailed occupant restraint system.

In this paper, the full-scale vehicle is impacted on a rigid wall with an initial velocity of 50 km/h according to the National Crash Legislation Configuration (GB11551-2003). The corresponding physical experiments have already been carried out. The physical model and FE model of full-scale vehicle are shown in Fig. 9.

2.4 Experimental validation of numerical models

Prior to any design optimization being performed from the simulation, the FE model needs to be validated with physical test. To systematically study the consistency between numerical simulation and physical experiment, the following criteria can be used: (a) the structural deformation pattern; (b) the matching degree of the overall shape of crash pulse between numerical simulation and physical test; and (c) the peak acceleration and the corresponding time. Figure 10 compares the structural deformation patterns between numerical simulations and the physical tests under full width frontal impact at t=0, t=30, t=60 and t=120 ms, respectively. Many of the characteristics observed in the tests are reproduced in the simulation. The overall collision response produces a pitching motion of the vehicle with a noticeable downward motion forward of the passenger compartment and a lifting of the rear of the vehicle. The hood is folded upward in the middle and the deformations are small in the vehicle behind the firewall. Obviously, the simulation results agree well with the corresponding snapshots of the physical test, which satisfies the first criterion of correlation aforementioned.

The deformation patterns of test and simulation for FLB are given in Fig. 11. It can be seen from Fig. 11 that relatively similar deformation patterns occur among

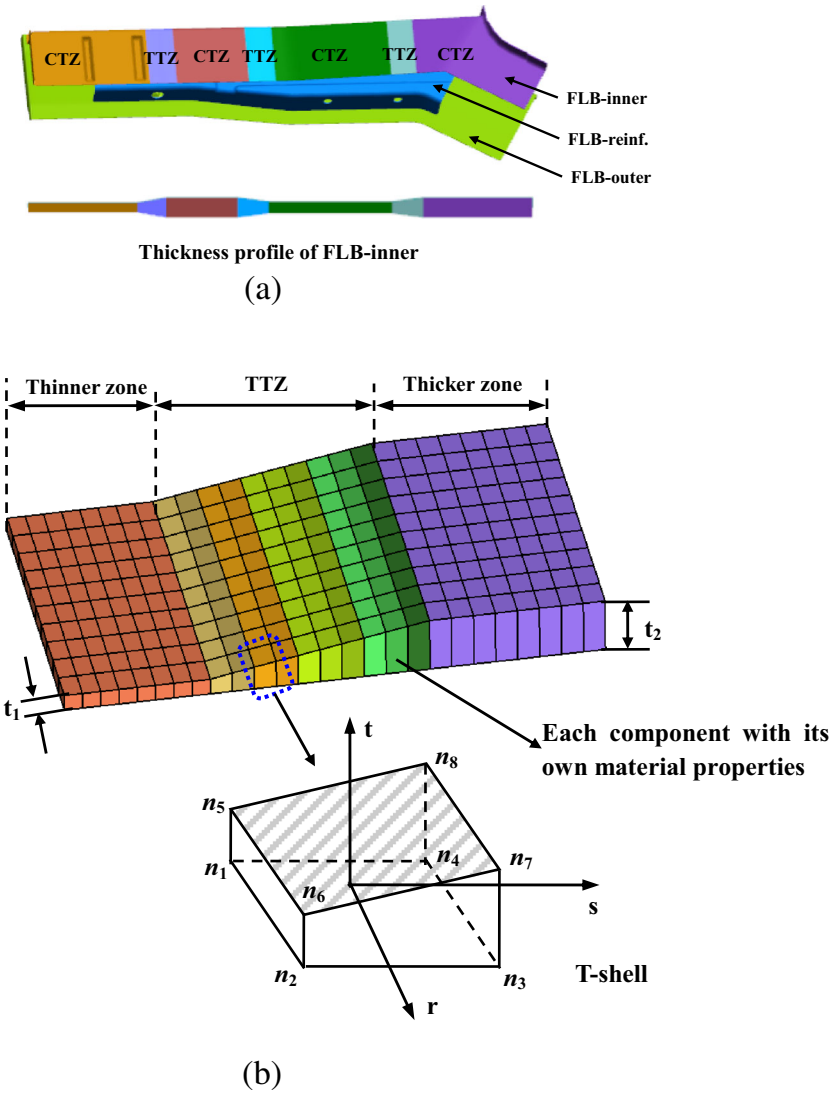

Fig. 8 (**a**) Geometry model of TRB FLB-inner; and (**b**) FE model of TRB

the simulation and the test. Figure 12 plots the acceleration histories of the simulation and test on the left sill at B-pillar level, which is a significant criterion to estimate the performance of vehicle crashworthiness. The pulses were filtered with CFC 60 Hz according to the standard of Society of Automotive Engineers (SAE) J211. It shows that there is good agreement on the peak accelerations and the corresponding times between the simulation and test of the full-scale vehicle.

To further verify the accuracy of numerical simulation, Table 2 summarizes the crashworthiness indicators between test and simulation. It can be seen that the simulation of the full-scale vehicle can capture the crashworthiness indicators of test in terms of peak acceleration and the corresponding time very well, FLB dynamic intrusion (Left and Right) and dash panel intrusion. According to the aforementioned analysis, the full-scale vehicle FE model can replace its physical model effectively to perform the subsequent design optimization.

3 Design optimization methodology

Though the TRB FLB-inner has excellent potential of lightweight and crashworthiness, it is not easy to obtain the optimal thickness distribution of TRB FLB-inner. Herein, structural optimization method is used to design the TRB FLB-inner. In the optimization progress, firstly, the conventional uniform thickness FLB-inner panel is replaced with the TRB. Secondly, optimal Latin hypercube sampling (OLHS) technique (Park 1994; Chen et al. 2006) is used to generate sampling points and the objective and constraints function values are

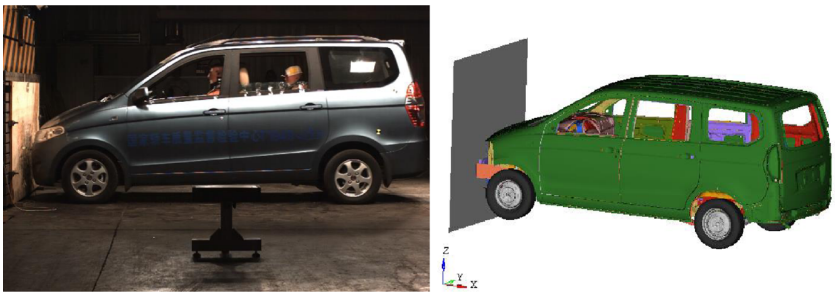

(a) (b)

Fig. 9 Physical model and FE model under full width frontal impact: (**a**) physical full-scale vehicle; (**b**) FE model of full-scale vehicle

(a) t=0ms

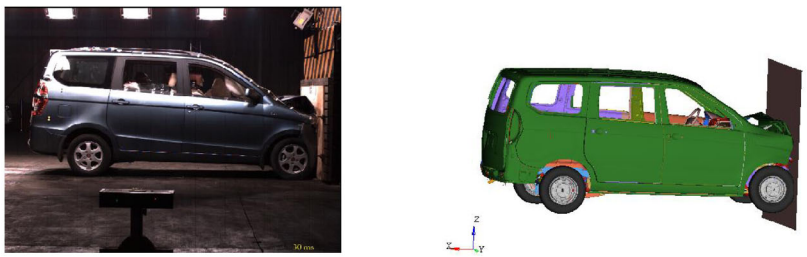

(c) t=30ms

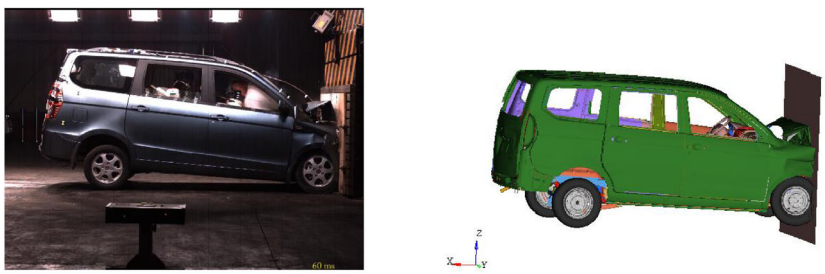

(d) t=60ms

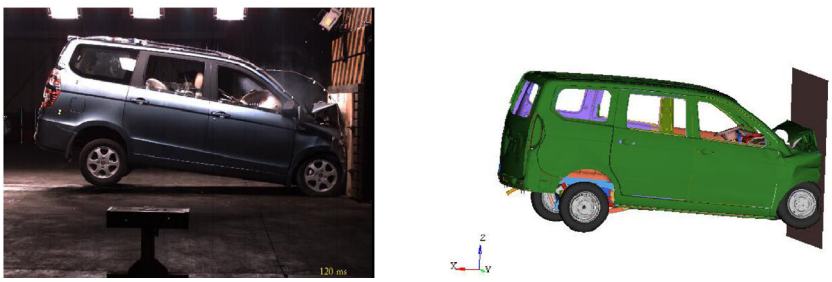

(e) t=120ms

Fig. 10 Comparison of deformation patterns between tests and numerical simulations

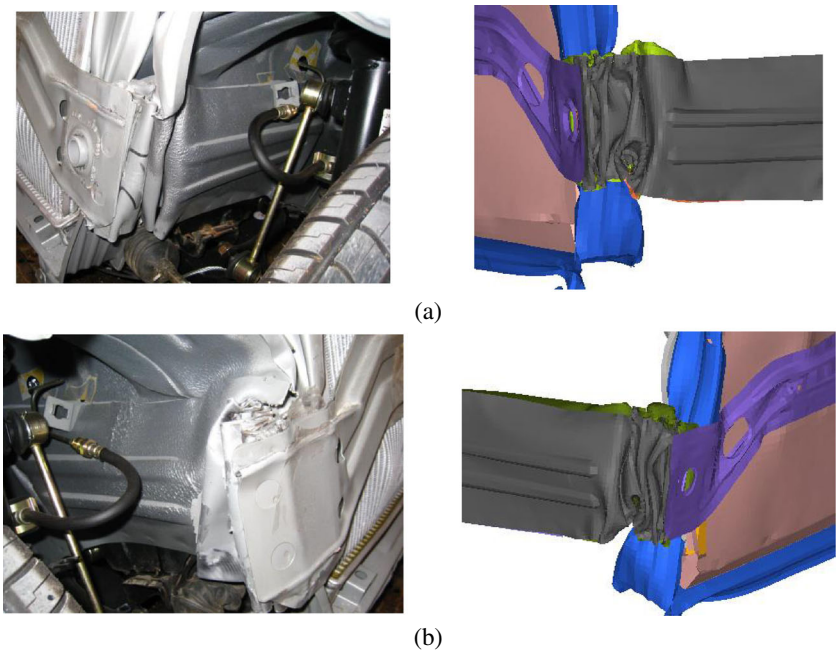

Fig. 11 Comparison of FLB deformation patterns between tests and numerical simulations: (**a**) Left FLB; (**b**) Right FLB

calculated using commercial software LS-DYNA. Following this, the ε-SVR technique (Vapnik 1995) is used to construct the surrogate models for the highly nonlinear impact responses. Finally, the Artificial Bee Colony (ABC) algorithm (Karaboga and Basturk 2007) is used to minimize the weight of TRB FLB-inner under the constraint of crashworthiness. The general formulation for this problem can be written as

$$\begin{cases} \underset{\boldsymbol{x}}{\text{Min}} & f(\boldsymbol{x}) \\ \text{s.t.} & g_j(\boldsymbol{x}) \geq 0, \quad j = 1, 2, \ldots q \\ & \boldsymbol{x}^L \leq \boldsymbol{x} \leq \boldsymbol{x}^U \end{cases} \tag{2}$$

where $f(\boldsymbol{x})$ is the objective function, $g_j(\boldsymbol{x})$ represents constraint functions, q is the number of constraints, $\boldsymbol{x}^L$ and $\boldsymbol{x}^U$ are the lower and upper bounds of the design vector $\boldsymbol{x}$, respectively.

3.1 ε-SVR metamodeling technique

Despite advances in computer throughput, the computational cost of complex high-fidelity engineering simulations often makes it impractical to rely exclusively on simulation for design optimization (Jin et al. 2001). Currently, many metamodeling techniques have been proposed to reduce the computational cost of expensive simulations of engineering problems, such as response surface models (RSM) (Engelund et al. 1993; Myers and Montgomery 1995), multivariate adaptive regression splines (MARS) (Friedman 1991), radial basis functions (RBF) (Hardy 1971; Dyn et al. 1986), and kriging models (KG) (Matheron 1963; Sacks et al. 1989; Kleijnen 2009), and a comparison of the four metamodeling techniques can be found in Ref. (Jin et al. 2001). All of these techniques are capable of function approximation, but they vary in their accuracy, robustness, computational efficiency and transparency. As an effective alternative, support vector regression (SVR) is a particular implementation of support vector machines (SVM) (Vapnik 1995), and it is a "very powerful method since its introduction has already outperformed most other systems in a wide variety of applications" (Cristianni and Shawe-Taylor 2000). The performance of the SVR was compared to that of the four metamodeling techniques commonly used in engineering design: RSM, MARS, RBF, and KG by Clarke and co-authors (2005). The results indicate that SVR has outperformed the four other approximation techniques in terms of accuracy and robustness, and that it provides a good compromise between prediction accuracy and robustness of a kriging model, with the computational efficiency and transparency near that of a RSM or RBF approximation (Clarke et al. 2005).

The SVR has different forms such as ε-support vector regression (ε-SVR) (Vapnik 1995) and ν-support vector regression (ν-SVR) (Schölkopf and Smola 2002). Among which, the ε-SVR is a promising metamodeling technique for function approximation of vehicle crash problems. It is widely used for function approximation of highly nonlinear crash problems (Zhu

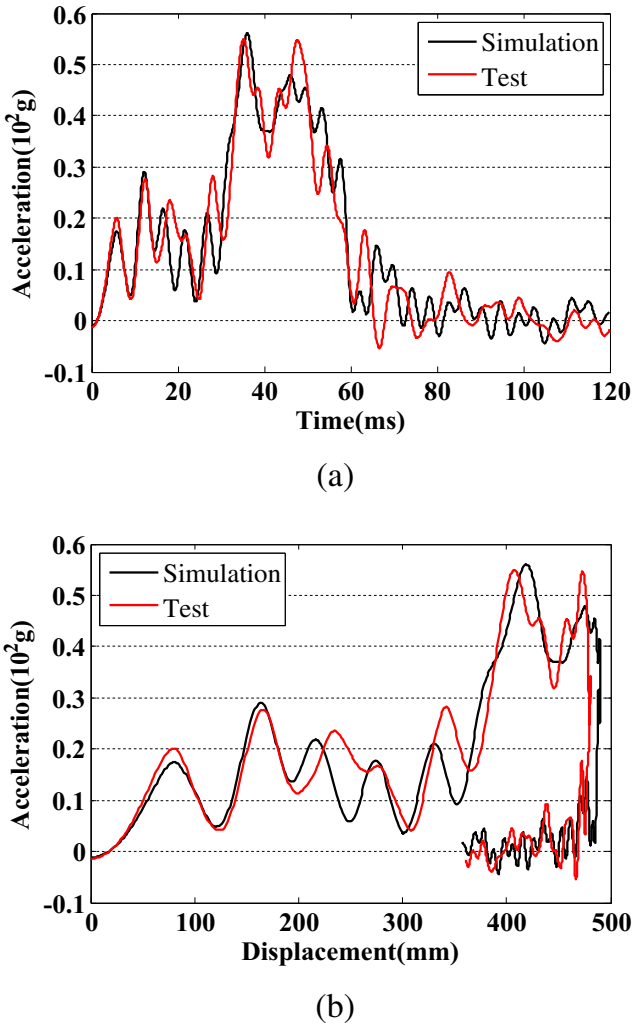

Fig. 12 Acceleration history on the left sill at B-pillar: (**a**) acceleration vs. time curve; and (**b**) acceleration vs. displacement curve

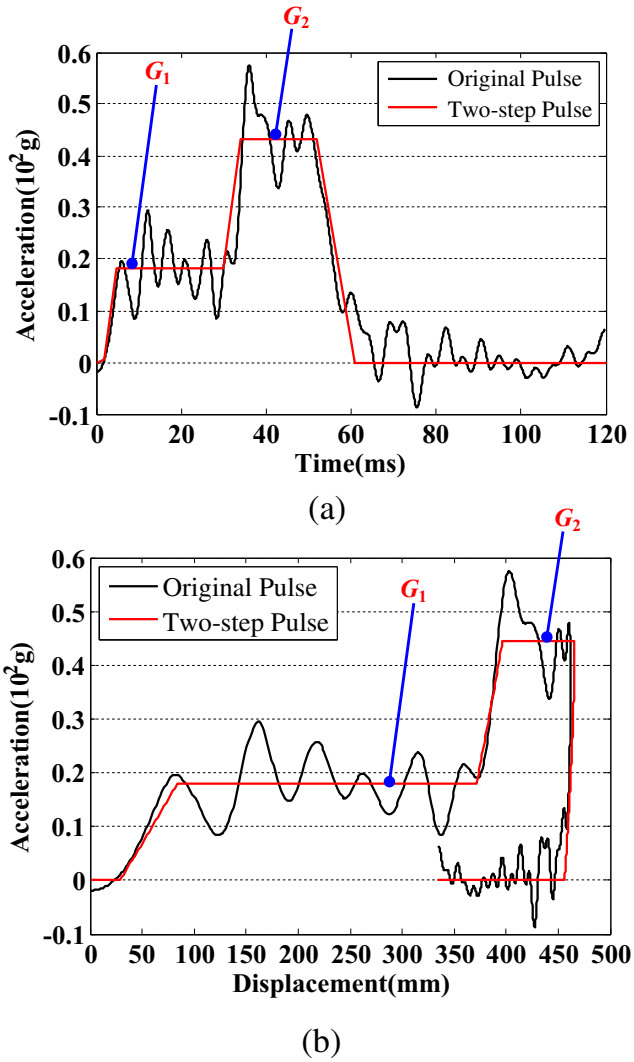

Fig. 13 Two-step crash pulse: (**a**) acceleration vs. time curve; and (**b**) acceleration vs. displacement curve

et al. 2009; Pan et al. 2010; Song et al. 2013). It maps data points from original design space to a higher dimensional characteristic space (Hilbert space) using a kernel function $k(\boldsymbol{x}_i, \boldsymbol{x}_j)$ and transforms nonlinear problems into linear divisible problems to obtain the optimum parameters of decision function (Vapnik 1995). A brief overview of ε-SVR is described in this section.

Table 2 Comparison of crashworthiness indicators between tests and simulations

Indicators		Test	Simulation
Peak acceleration (g)		54.94	56.01
Corresponding time of peak acceleration (ms)		35.20	36.09
Dash panel intrusion (mm)		130.56	133.81
FLB dynamic intrusion	Left (mm)	205.35	210.38
	Right (mm)	197.67	204.75

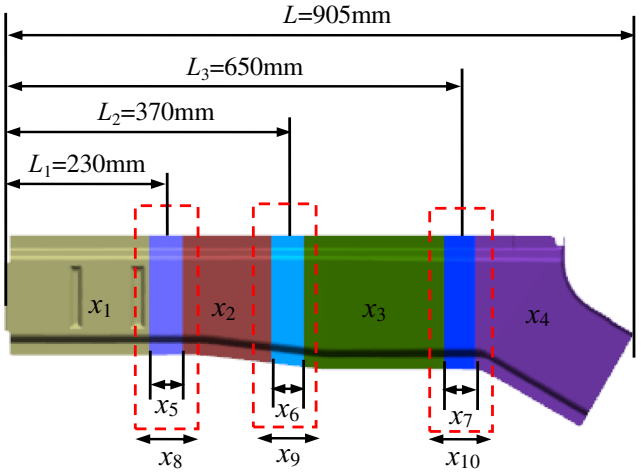

Fig. 14 Geometry parameters of FLB-inner structure

Table 3 Geometry parameters of FLB-inner for dynamic impact (Unit: mm)

Symbol	Lower bound	Upper bound	Baseline
x_1	1.0	2.0	1.6
x_2	1.0	2.0	1.6
x_3	1.0	2.0	1.6
x_4	1.0	2.0	1.6
x_5	$Max(40, 100*(x_2-x_1))$	120.0	40.0
x_6	$Max(40, 100*(x_3-x_2))$	120.0	40.0
x_7	$Max(40, 100*(x_4-x_3))$	120.0	40.0
x_8	150.0	260.0	230.0
x_9	330.0	410.0	370.0
x_{10}	570.0	690.0	650.0

Given a set of training data, $\{(\boldsymbol{x}_1, y_1),\ldots,(\boldsymbol{x}_N, y_N)\}$, such that $\boldsymbol{x}_i \in R^N$ is a training vector and $y_i \in R^N$ is a target output, the standard form of nonlinear ε-SVR (Vapnik 1998) is

$$\begin{cases} \min\limits_{w,b,\boldsymbol{\xi},\boldsymbol{\xi}^*} & \frac{1}{2}\boldsymbol{w}^T\boldsymbol{w} + C\sum\limits_{i=1}^{N}\xi_i + C\sum\limits_{i=1}^{N}\xi_i^* \\ \text{subject to} & \boldsymbol{w}^T\,\Phi(\boldsymbol{x}_i) + b - y_i \le \varepsilon + \xi_i, \\ & y_i - \boldsymbol{w}^T\,\Phi(\boldsymbol{x}_i) - b \le \varepsilon + \xi_i^*, \\ & \xi_i,\ \xi_i^* \ge 0,\ i = 1, \cdots, N \end{cases} \tag{3}$$

After applying Lagrange function, the dual form of the original optimization problem can be written as

$$\begin{cases} \min\limits_{\alpha,\alpha^*} & \frac{1}{2}\sum\limits_{i,j=1}^{N}(\alpha_i-\alpha_i^*)(\alpha_j-\alpha_j^*)k(\boldsymbol{x}_i,\boldsymbol{x}_j) + \varepsilon\sum\limits_{i=1}^{N}(\alpha_i+\alpha_i^*) + \sum\limits_{i=1}^{N}y_i(\alpha_i-\alpha_i^*) \\ \text{subject to} & \sum\limits_{i=1}^{N}(\alpha_i-\alpha_i^*) = 0, \\ & 0 \le \alpha_i,\ \alpha_i^* \le C,\ i = 1, \cdots, N \end{cases} \tag{4}$$

where N is the number of sample points, α_i and α_i^* are the Lagrange multiplier respectively, $C>0$ is the penalty factor of error term, $\boldsymbol{\xi}$ and $\boldsymbol{\xi}^*$ are the slack variables, $\varepsilon>0$ is insensitive loss function which controls the number of support vectors and $k(\boldsymbol{x}_i, \boldsymbol{x}_j) \equiv \Phi(\boldsymbol{x}_i)^T\Phi(\boldsymbol{x}_j)$ is kernel function, which is here a N by N positive semi-definite matrix.

In this paper, the Gaussian kernel function $k(\boldsymbol{x}_i, \boldsymbol{x}_j)$ is adopted in ε-SVR and its form can be written as

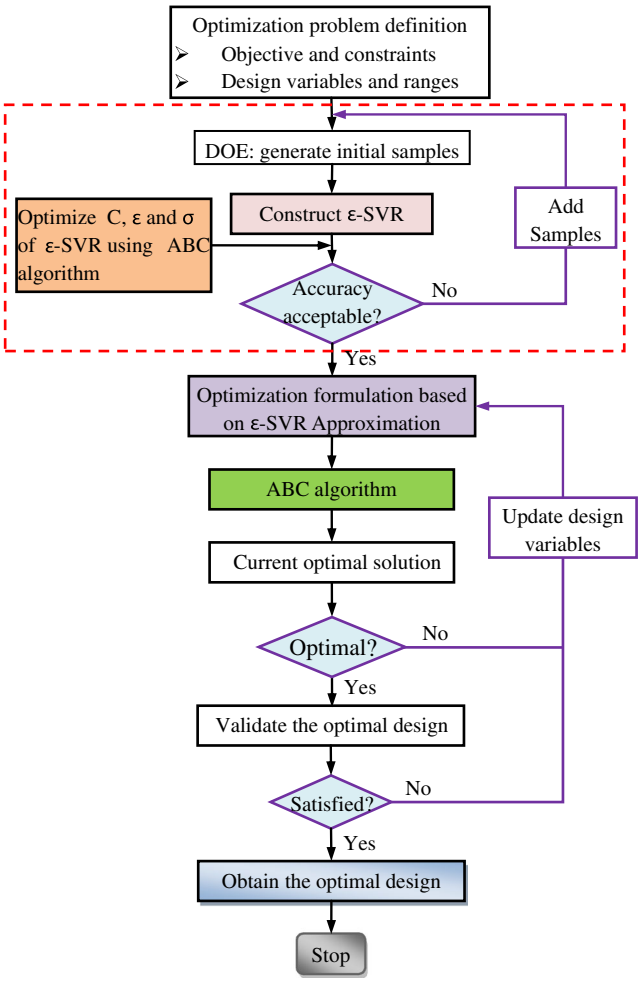

Fig. 15 Flowchart of optimization process

Table 4 Design requirements and targets

Indicators		Symbol	Baseline	Target
Peak acceleration (g)		$A(x)$	56.01	≤55
The first-step acceleration (g)		$G_1(x)$	14.47	≥15
The second-step acceleration (g)		$G_2(x)$	43.85	≤42
Energy absorption of FLB (J)		$E(x)$	61,002.69	≥62,000
Dash panel intrusion (mm)		$S_1(x)$	133.81	≤120
FLB dynamic intrusion	Left (mm)	$S_2(x)$	210.38	≥215
	Right (mm)	$S_3(x)$	204.75	≥215

Table 5 Optimal parameters and error analysis of ε-SVRs

Responses	C	ε	σ	R^2_{CV-5}	$RMSE_{CV-5}$
$M(x)$	74.1409	0.0121	15.4374	0.9996	0.0087
$A(x)$	31.1739	0.4254	1.0841	0.9891	0.0107
G_1	20.5431	0.0685	14.2003	0.9802	0.0582
G_2	55.0406	0.2744	1.3499	0.9953	0.0115
$E(x)$	6.0373	0.0102	6.9999	0.9810	0.0596
$S_1(x)$	54.2321	0.3266	1.2372	0.9979	0.0101
$S_2(x)$	24.2425	0.2819	1.3318	0.9849	0.0403
$S_3(x)$	0.3877	0.0143	0.0890	0.9854	0.0134

Table 6 Detail parameters of ABC algorithm used in this study

ABC parameter name	Values
Number of colony size	20
Number of food sources	10
"limit" trials	100
Max iterations	100
Tolerance	1*e-6

(Vapnik 1995, 1998; Cherkassky and Mulier 1998; Schölkopf et al. 2002):

$$k(\boldsymbol{x}_i,\boldsymbol{x}_j)=\exp\left(-\frac{\|\boldsymbol{x}_i-\boldsymbol{x}_j\|^2}{2\sigma^2}\right) \tag{5}$$

The optimal $\overline{\alpha}_i$ and $\overline{\alpha}_i^*$ are obtained through solving the optimization problem of the (4). The decision function of the ε-SVR is then written as

$$f(\mathbf{x})=\sum_{i=1}^{n}\left(\overline{\alpha}_i^*-\overline{\alpha}_i\right)k(\boldsymbol{x}_i,\boldsymbol{x})+\overline{b} \tag{6}$$

The optimal $\overline{b}$ can thus be formulated as

$$\overline{b}=y_j-\sum_{i=1}^{n}\left(\overline{\alpha}_i^*-\overline{\alpha}_i\right)k(\boldsymbol{x}_i,\boldsymbol{x}_j)+\varepsilon,\forall j\in\left\{j|0<\overline{\alpha}_j<C\right\} \tag{7}$$

As the regression accuracy of ε-SVR mainly depends on values of C, ε and Gaussian kernel parameter σ, the ABC algorithm described in Section 3.2 is used to search the optimal values of C, ε and σ to obtain the best regression effect with limited samples. Due to the computational cost of estimating the prediction accuracy of surrogate models, cross-validation (CV) is often used as an alternative for assessing accuracy (Viana et al. 2009). The idea of CV for assessing accuracy is to estimate the risk of the considered estimator on surrogate models by using a repeated data-splitting scheme. It is attractive because it does not depend on the statistical assumptions of a particular surrogate technique and it does not require extra test points (Varma and Simon 2006). Consequently, the interest of CV is that it is based on a heuristic that can be applied with great universality. Many data-splitting rules have been proposed, such as leave-one-out (Allen 1974) and k-fold cross-validation (Kohavi 1995; Browne 2000) etc. The leave-one-out strategy is computationally expensive for large number of points. A variation of the k-fold strategy is then applied in this paper to overcome this problem. According to the classical k-fold strategy, the training set is divided into k disjoint folds of equal size randomly. One fold is recognized as the validation set and the remaining folds are recognized as the training set. The CV process is then repeated k times with each of the k folds used exactly once as validation data. In this paper, 5-fold cross-validation is adopted to evaluate the prediction accuracy of ε-SVR. Typically, the squared correlation coefficient R^2_{CV-5} and the root mean square error ($RMSE_{CV-5}$) (Liao et al. 2008; Hou et al. 2008) are respectively defined as the cross validation accuracy. Note that the larger the value of R^2_{CV-5} is, as well as the smaller the value of $RMSE$, the higher prediction

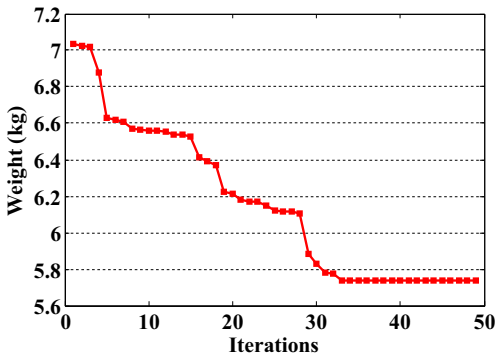

Fig. 16 Iterations process of the weight of TRB FLB-inner

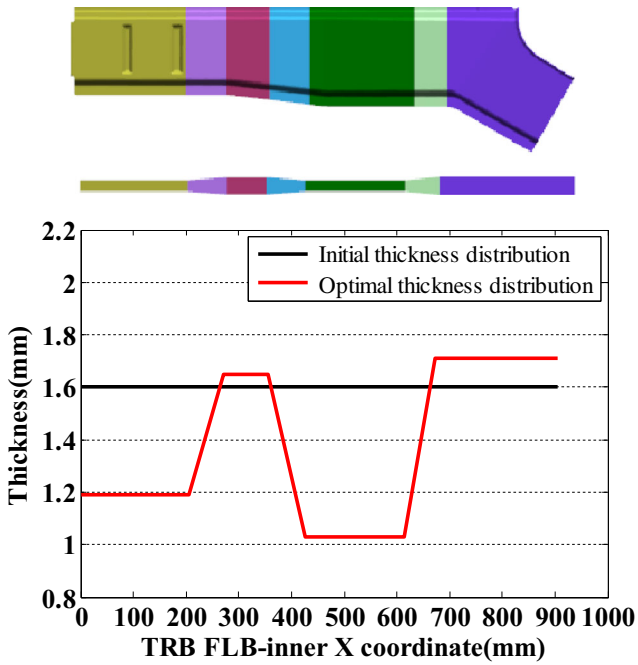

Fig. 17 Thickness profile of TRB FLB-inner

Table 7 Optimization of design variables

Description	x_1	x_2	x_3	x_4	x_5	x_6	x_7	x_8	x_9	x_{10}
Baseline	1.60	1.60	1.60	1.60	40.0	40.0	40.0	230.0	370.0	650.0
Optimum	1.19	1.65	1.03	1.71	75.1	70.8	59.5	243.1	391.3	642.8

accuracy for ε-SVR meta-model becomes. The formulations of these criteria are as follows

$$R^2_{CV-5} = \frac{1}{5}\sum_{j=1}^{5}\left(1-\frac{\sum_{i=1}^{l}\left(y_i-\hat{y}_i\right)^2}{\sum_{i=1}^{l}\left(y_i-\overline{y}_i\right)^2}\right) \tag{8}$$

$$RMSE_{CV-5} = \frac{1}{5}\sum_{j=1}^{5}\sqrt{\frac{1}{l}\sum_{i=1}^{l}\left(y_i-\hat{y}_i\right)^2} \tag{9}$$

where l is the number of data points at each validation set, y_i is the observed response value, $\hat{y}_i$ is the predicted value and $\overline{y}$ is the mean value of y_i, respectively.

3.2 Artificial bee colony (ABC) algorithm

Recently, the ABC algorithm has drawn increasing attention for its high performance to solve various engineering problems. Karaboga and Basturk (2007) compared the performance of the ABC algorithm with that of Genetic Algorithm (GA) (Goldberg 1989), Particle Swarm Algorithm (PSO) (Poli et al. 2007; Kennedy and Eberhart 1995) and Particle Swarm Inspired Evolutionary Algorithm (PS-EA) (Srinivasan and Seow 2003) using five high dimensional numerical benchmark functions that have multimodality. The results showed that ABC algorithm outperforms the other algorithms. In the latter literature (Karaboga and Basturk 2008; Karaboga and Akay 2009; Singh 2009; Akay and Karaboga 2012), the ABC algorithm is further proved comparable to differential evolution (DE) (Storn and Price 1997) and PSO for multi-dimensional numerical problems and is proved that the ABC algorithm can be employed to solve engineering problems with high dimensionality. It is noted that ABC has been employed successfully to solve the design problems of sheet metal forming (Sun et al. 2012). Therefore, the ABC algorithm is used as an optimizer for crashworthiness design of the FLB-inner in this study. The features of the ABC algorithm will be described as follows.

The ABC algorithm, proposed and further developed by Karaboga and coauthors (Karaboga and Basturk 2007, 2008; Karaboga and Akay 2009), is a swarm based meta-heuristic algorithm for numerical optimization problems. It is motivated by the intelligent foraging behavior of honey bees. In the ABC algorithm, the position of a food source represents a possible solution of the optimization problem and the nectar amount of a food source corresponds to the quality (fitness) of the associated solution. The number of the employed bees or the onlooker bees is equal to the number of solutions in the population. The aims of the artificial bees are to find the positions of food sources with high nectar amount. If the nectar amount of a new source is higher than that of the previous one in their memory, the position of the food source is updated until the best position is found. The more details of the ABC algorithm can be consulted from literature (Karaboga and Basturk 2007, 2008; Karaboga and Akay 2009).

4 Design optimization and results analysis

4.1 Design responses and variables

Crash pulse is one of the most significant factors to describe vehicle crash behavior. However, as the crash pulse is full of

Table 8 Error analysis of the optimal solution

Indicators		Symbol	Design optimization		
			Optimum	FE model	Error (%)
Weight (kg)		$M(x)$	5.68	5.74	−1.05 %
Peak acceleration (g)		$A(x)$	51.85	52.49	−1.22 %
The first-step acceleration (g)		$G_1(x)$	16.83	16.15	4.21 %
The second-step acceleration (g)		$G_2(x)$	41.05	41.87	−1.96 %
Energy absorption of FLB (J)		$E(x)$	64,186.82	63,572.75	0.97 %
Dash panel intrusion (mm)		$S_1(x)$	106.47	102.34	4.04 %
FLB dynamic intrusion	Left (mm)	$S_2(x)$	230.29	233.52	−1.38 %
	Right (mm)	$S_3(x)$	232.47	236.62	−1.76 %

Table 9 Improvements of vehicle performance for lightweight design optimization

Description	Baseline design	Optimal design	Improvement (%)
$M(x)$	6.77 (kg)	5.74 (kg)	−15.21 %
$A(x)$	56.01 (g)	52.49 (g)	−6.28 %
$G_1(x)$	14.47 (g)	16.15 (g)	11.61 %
$G_2(x)$	43.85 (g)	41.87 (g)	−4.52 %
$E(x)$	61,002.69 (J)	63,572.75 (J)	4.21 %
$S_1(x)$	133.81 (mm)	102.34 (mm)	−23.52 %
$S_2(x)$	210.38 (mm)	233.52 (mm)	10.99 %
$S_3(x)$	204.75 (mm)	236.62 (mm)	15.57 %

Noted: Improvement $= \frac{\text{Optimal design-Baseline design}}{\text{Baseline design}} \times 100\%$

oscillations, it is hard to intuitively make the point-wise comparison for different designs and hard to describe the engineering judgments analytically. Fortunately, the crash pulse of vehicle with front-engine can be simplified as two-step pulse which provides an effort to simulate this complex process by averaging and smoothing the data in a systematic and objective way, as shown in Fig. 13. In the first step (G_1), the FLB buckles in a desired folding pattern. Correspondingly the crash pulse presents an oscillation around a plateau. In the second step (G_2), more parts such as middle rail, sled runner etc. become loaded and buckled. The engine block will impact the dash panel. The crash pulse presents another period of oscillation around a second plateau. The simplified two-step crash pulse was shown to have negligible errors on the occupant response values (Wu et al. 2001). Therefore, the two-step pulse is adopted in this study to quantify the actual crash pulse curve with few parameters such as G_1 and G_2. Generally, in order to obtain good occupant protection response values, designers usually expect increasing the first-step acceleration G_1 and decreasing the second-step acceleration G_2, respectively, without losing the living space of the passenger compartment.

Besides the peak acceleration, the crashworthiness of FLB can be evaluated by energy absorption, dash panel intrusion and FLB dynamic intrusion (Left and Right) (Zhang et al. 2007; Zhu et al. 2009; Pan and Zhu 2011; Gu et al. 2013). Hence, peak acceleration, energy absorption and intrusion are chosen as the vehicle crashworthiness indicators (see Table 4), represented by $A(x)$, $E(x)$ $S_1(x)$, $S_2(x)$ and $S_3(x)$, respectively. In addition, the first-step acceleration $G_1(x)$ and the second-step acceleration $G_2(x)$ are also considered as constraint functions. The weight of the TRB FLB-inner is regarded as the objective function, denoted by $M(x)$.

According to engineering experience, the lightweight and crashworthiness potential of TRB structure can be fully exploited through optimizing the following three kinds of parameters: (a) thicknesses of constant thickness zone (CTZ), (b) length of thickness transition zone (TTZ) and (c) position of TTZ. Considering the TRB manufacturing capacity of BAOSTEEL CO., LTD, two additively conditions are imposed to ensure the rollability: (1) the ratio of maximum and minimum thickness within the same TRB part must vary within 2:1; (2) the transition slope must vary with 1:100, which means 1 mm thickness difference over a length of 100 mm.

Considering structural symmetry of TRB FLB-inner, thicknesses (x_1~x_4) of CTZ, length (x_5~x_7) and position (x_8~x_{10}) of TTZ are chosen as design variables in this study, see Fig. 14. Table 3 shows the range and the baseline value of each design variable. The ranges of the variables are defined according to engineering experience and the TRB manufacturing capacity of BAOSTEEL CO., LTD.

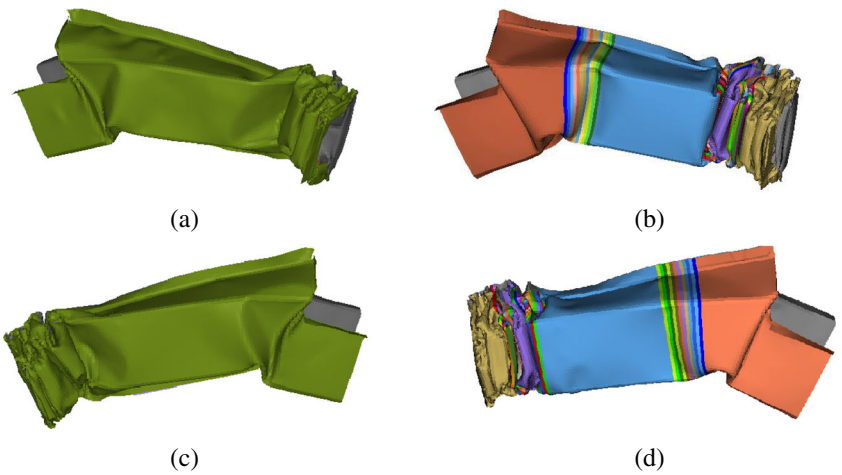

Fig. 18 Comparison of the numerical result before and after optimization: (**a**) left FLB of baseline design; (**b**) left FLB of optimal design; (**c**) right FLB of baseline design; and (**d**) right FLB of optimal design

4.2 Optimization problem formulation

The baseline design and the design target are listed in Table 4. The structural crashworthiness performance of the simplified frontal impact model should be no worse than that of the baseline design. Therefore, the design optimization for the TRB FLB-inner can be formulated as follows:

$$\begin{cases} \min & M(\boldsymbol{x}) \\ s.t. & A(\boldsymbol{x}) \le 55 \ \text{g} \\ & G_1(\boldsymbol{x}) \ge 15\ g \\ & G_2(\boldsymbol{x}) \le 42\ g \\ & E(\boldsymbol{x}) \ge 62000 \ \text{J} \\ & S_1(\boldsymbol{x}) \le 120 \ mm \\ & S_2(\boldsymbol{x}) \ge 215 \ mm \\ & S_3(\boldsymbol{x}) \ge 215 \ mm \\ & \boldsymbol{x}^L \le \boldsymbol{x} \le \boldsymbol{x}^U,\ \boldsymbol{x} = (x_1,\ x_2,\ x_3, x_4, x_5, x_6, x_7, x_8, x_9, x_{10})^T \end{cases} \tag{10}$$

4.3 Optimization problem process

The whole design process of the TRB FLB-inner under crashworthiness is given in a flowchart, as shown in Fig. 15. Considering the large computational burden of the FE runs, OLHS technique is adopted to generate 300 sampling points in the whole design space. The objective and constraints function values are calculated using commercial software LS-DYNA. The ε-SVR technique is then used to construct the surrogate models for $M(x)$, $A(x)$, $G_1(x)$, $G_2(x)$, $E(x)$, $S_1(x)$, $S_2(x)$ and $S_3(x)$, respectively. In this paper, the initial values of C, ε and σ of ε-SVR are respectively set to 1, 0.1 and $\sqrt{n/2}$, where n is the number of design variables, $C \in (0.1, 100)$, $\varepsilon \in (0.01, 1)$ and $\sigma \in (0.05, 25)$. The ABC algorithm is then used to search the optimal values of C, ε and σ for each output response to obtain the best regression effect with the limited samples. Table 5 lists the optimal parameters and the cross-validation accuracy of the ε-SVRs, which appear reasonably accurate for the design optimization.

Finally, the ABC algorithm is used to perform lightweight design optimization based on these ε-SVR surrogate models. The parameters of ABC algorithm are summarized in Table 6.

In Table 6, colony size is the number of employed bees and onlooker bees; the number of food sources equals the half of the colony size; "limit" trials hold trial numbers through which solutions cannot be improved; the parameter "Max iterations" is the number of cycles for foraging, which is a stopping criterion; the parameter "Tolerance" is another stopping criterion, it controls the convergence speed and search accuracy.

When the number of iterations achieves its max iterations or the increment of the mean of the last five

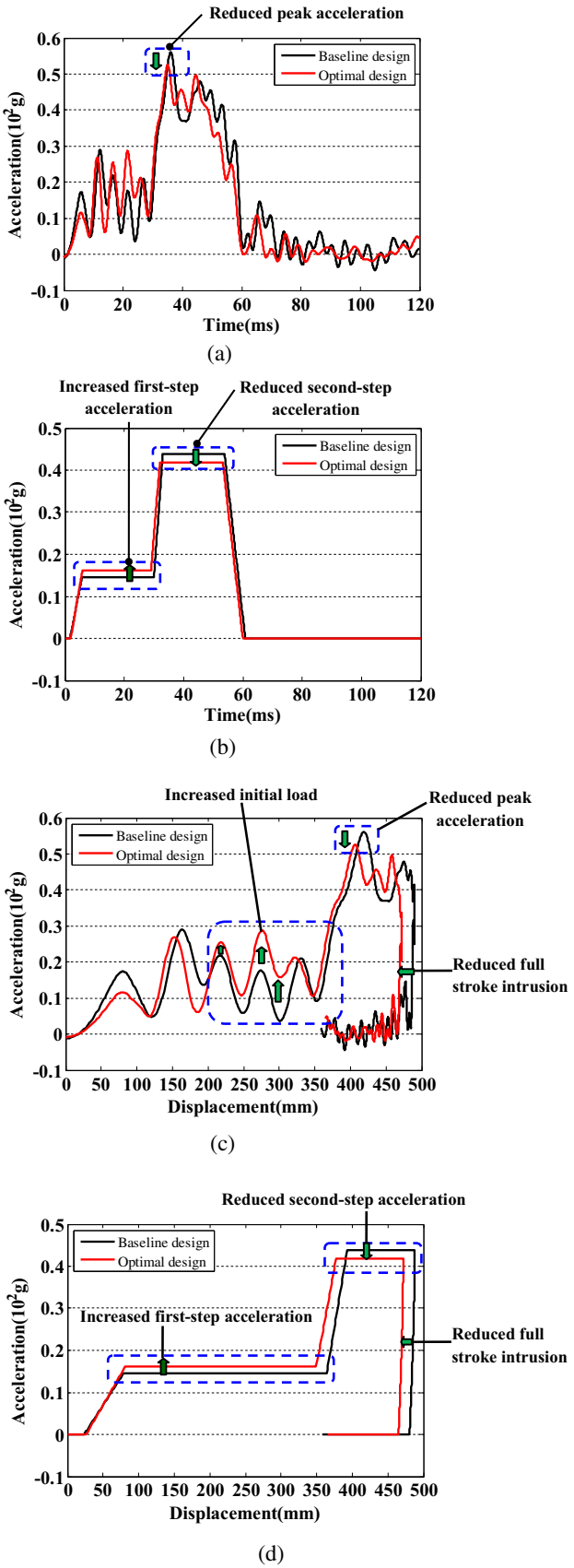

Fig. 19 Comparison of crash pulses before and after optimization

smallest objective function values becomes negligible, the search process will be terminated (see (11)).

$$\begin{cases} \left|\overline{F_{i+1}}-\overline{F_i}\right| \le \varepsilon,\ i = 1, 2, \ldots, n \\ \overline{F_i} = \dfrac{\sum_{j=1}^{5} f_j}{5} \end{cases} \tag{11}$$

where ε is the tolerance in the ABC algorithm (1*e-6 used in this paper), f_j is the jth smallest objective function value.

The iterative process of $M(x)$ is shown in Fig. 16. From which, it is easily found that the optimization progress converged after 33 iterations. The optimal results are listed in Table 7 and the corresponding thickness profile of the TRB FLB-inner is shown in Fig. 17.

The relative errors of the optimal solution are listed in Table 8. Obviously, the optimal solution generated from the surrogate models has sufficient accuracy compared with the FE simulation results. It is proved once again that the effectiveness of the design method. The results of the FE simulation are chosen as the optimal solution in this study.

The improvements of crashworthiness of FLB-TRB with respect to baseline design are listed in Table 9. From which, it is easily found that the weight reduction achieves 15.21 % and the energy absorption of FLB increases by 4.21 % relative to the baseline design, respectively. In addition, the peak acceleration, the second step acceleration (G_2) and the firewall intrusion of the optimal design have been decreased by 6.28 and 4.52 and 23.52 %, respectively.

Figure 18 compares the deformation patterns of the FLB before and after optimization. From which, it is easily found that the deformation patterns of the FLB can be greatly improved through the redistribution of thickness of the FLB-inner. Figure 19 depicts the numerical results of crash pulses for the baseline and optimal design. In the baseline design, the 'space B' of the FLB buckled sideway, which leads to a sharp drop of crash loading until 30 ms and the 'space D' happened sharp bending deformation, which greatly decreases the resistance load of the FLB. In the optimal design, the 'space A' and 'space B' have relatively uniform and progressive axial collapse, the previous sharp bending deformation is disappeared in the 'space D', which leads to the increment of the first-step acceleration G_1, as well as the reduction of peak acceleration and the second-step acceleration G_2.

Figure 20 plots the dash panel intrusion contour of passenger car under full width frontal impact before and after optimization. The maximum intrusion of dash panel decreases a bit when using an optimized TRB FLB-inner. For the baseline design, the maximum dash panel intrusion is 133.81 mm, while for the passenger car model with optimized TRB FLB-inner, the maximum dash panel intrusion value is 102.34 mm. The results showed that optimal thickness distribution of the TRB FLB-inner can not only reduce its weight remarkably but also enhance vehicle crashworthiness.

5 Conclusions and further work

Aiming at achieving the maximum weight reduction of vehicle structures, lightweight design of FLB-inner by using TRB technique has been successfully performed under frontal impact in this study. The FLB-inner is divided into four different thickness segments according to the performance requirements. The material constitutive model of TRB is established through using the piecewise linear interpolation method. The FE model of TRB FLB-inner is simulated by using 8-nodes thick shell elements (T-shell in LS-DYNA). The ε-SVR metamodels are used to approximate the crashworthiness responses and the ABC algorithm is applied to search for the optimum. The optimal solution shows that the weight of FLB-inner is reduced by 15.21 %, while the energy absorption of FLB increased by 4.21 %, the peak acceleration reduced by 6.28 %, the first step acceleration (G_1) increased by 11.61 %, the second step acceleration (G_2) reduced by 4.52 % and dash panel intrusion reduced by 23.52 %, respectively. It is clearly shown that the TRB technique has great potential to realize lightweight and have great application prospect in the vehicle industry.

This study is conducted under only one crash load-case. However, the real vehicle crash scenario usually involves

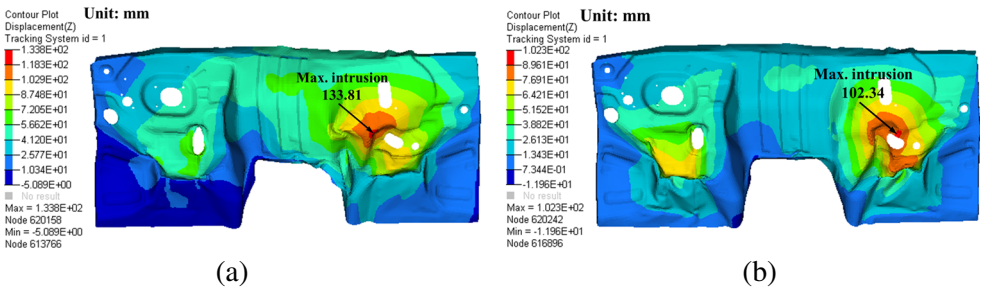

Fig. 20 Comparison of dash panel intrusion contour before and after optimization: (**a**) baseline design; and (**b**) optimal design

various crash load-cases, such as full width frontal impact, 40 % offset impact, small offset impact and side impact etc. The designers often consider these crash load-cases simultaneously in the development of vehicle product. Hence, future research needs to combine MDO (Chuang et al. 2008) or multiobjective optimization methodology (Xiao et al. 2015) for the lightweight and crashworthiness design of vehicle structures by using TRB technique.

Acknowledgments This work was supported from The Key Project of National Natural Science Foundation of China (61232014) and the Program of NSFC of China (11202072), The Doctoral Fund of Ministry of Education of China (20120161120005), The Open Fund Program of the State Key Laboratory of Vehicle Light-weight Design, P. R. China (20130303) and the Hunan Provincial Science Foundation of China (13JJ4036).

References

Akay B, Karaboga D (2012) Artificial bee colony algorithm for large-scale problems and engineering design optimization. J Intell Manuf 23(4):1001–1014

Allen DM (1974) The relationship between variable selection and data augmentation and a method for prediction. Technometrics 16(1): 125–127

Beiter P, Groche P (2011) On the development of novel light weight profiles for automotive industries by roll forming of tailor rolled blanks. Key Eng Mater 473:45–52

Browne MW (2000) Cross-validation methods. J Math Psychol 44(1): 108–132

Chen VCP, Tsui KL, Barton RR, Meckesheimer M (2006) A review on design, modeling and applications of computer experiments. IIE Trans 38(4):273–291

Cherkassky V, Mulier F (1998) Learning from data: concepts, theory. Wiley, New York

Chuang CH, Yang RJ, Li G, Mallela K, Pothuraju P (2008) Multidisciplinary design optimization on vehicle tailor rolled blank design. Struct Multidiscip Optim 35(6):551–560

Clarke SM, Griebsch JH, Simpson TW (2005) Analysis of support vector regression for approximation of complex engineering analyses. J Mech Des 127(6):1077–1087

Cristianni N, Shawe-Taylor J (2000) An introduction to support vector machines and other Kernel-based learning methods. Cambridge University Press, Cambridge

Dyn N, Levin D, Rippa S (1986) Numerical procedures for surface fitting of scattered data by radial basis functions. SIAM J Sci Stat Comput 7(2):639–659

Engelund WC, Douglas OS, Lepsch RA, McMillian MM, Unal R (1993) Aerodynamic configuration design using response surface methodology analysis. AIAA, Aircraft Design, Systems and Operations Meeting, Monterey, CA, Aug. 11–13

Friedman JH (1991) Multivariate adaptive regression splines. Ann Stat 19(1):1–141

Future Steel Vehicle - Final Engineering Report, www.worldautosteel.org (5/17/2011)

Goede M, Stehlin M, Rafflenbeul L, Kopp G, Beeh E (2009) Super light car-lightweight construction thanks to a multi-material design and function integration. Eur Transp Res Rev 1(1):15–20

Goldberg DE (1989) Genetic algorithms in search, optimization and machine learning. Addison-Wisely, MA

Gu GX, Sun GY, Li GY, Mao LC, Li Q (2013) A Comparative study on multiobjective reliable and robust optimization for crashworthiness design of vehicle structure. Struct Multidiscip Optim 48:669–684

Halquist J (2007) LS-DYNA keyword user's manual version 971. Livermore Software Technology Corporation, Livermore

Hardy RL (1971) Multiquadratic equations of topography and other irregular surfaces. J Geophys Res 76:1905–1915

Hirt G, Dávalos-Julca DH (2012) Tailored profiles made of tailor rolled strips by roll forming - part 1 of 2. Steel Res Int 83(1):100–105

Hou SJ, Li Q, Long SY, Yang XJ, Li W (2008) Multiobjective optimization of multi-cell sections for the crashworthiness design. Int J Impact Eng 35(12):1355–1367

Jeon SJ, Lee MY, Kim BM (2011) Development of automotive door inner panel using AA 5J32 tailor rolled blank. Trans Mater Process 20(7): 512–517

Jin R, Chen W, Simpson TW (2001) Comparative studies of metamodeling techniques under multiple modeling criteria. Struct Multidiscip Optim 23(1):1–13

Karaboga D, Akay B (2009) A comparative study of artificial bee colony algorithm. Appl Math Comput 214(1):108–132

Karaboga D, Basturk B (2007) A powerful and efficient algorithm for numerical function optimization: artificial bee colony (ABC) algorithm. J Glob Optim 39(3):459–471

Karaboga D, Basturk B (2008) On the performance of artificial bee colony (ABC) algorithm. Appl Soft Comput 8(1):687–697

Kennedy J, Eberhart RC (1995) Particle swarm optimization. In Proceedings of the 1995 I.E. International Conference on Neural Networks (4): 1942–1948

Kleijnen JP (2009) Kriging metamodeling in simulation: a review. Eur J Oper Res 192(3):707–716

Kohavi R (1995) A study of cross-validation and bootstrap for accuracy estimation and model selection. In: International Joint Conference on Artificial Intelligence, pp 1137–1143

Kopp R, Wiedner C, Meyer A (2005a) Flexibly rolled sheet metal and its use in sheet metal forming. Adv Mater Res 6–8:81–92

Kopp R, Wiedner C, Meyar A (2005b) Flexible rolling for load-adapted blanks. Int Sheet Metal Rev 7(4):20–24

Li Y, Lin Z, Jiang A, Chen G (2003) Use of high strength steel sheet for lightweight and crashworthy car body. Mater Des 24(3):177–182

Li GY, Xu FX, Huang XD, Sun GY (2015a) Topology optimization of an automotive tailor-welded blank door. J Mech Des 137(5):055001

Li GY, Xu FX, Sun GY, Li Q (2015b) A comparative study on thin-walled structures with functionally graded thickness (FGT) and tapered tubes withstanding oblique impact loading. Int J Impact Eng 77:68–83

Liao XT, Li Q, Yang XJ, Zhang WG, Li W (2008) Multi-objective optimization for crash safety design of vehicles using stepwise regression model. Struct Multidiscip Optim 35(6):561–569

Matheron G (1963) Principles of geostatistics. Econ Geol 58(8):1246–1266

Meyer A, Wietbrock B, Hirt G (2008) Increasing of the drawing depth using tailor rolled blanks-numerical and experimental analysis. Int J Mach Tools Manuf 48(5):522–531

Muhr und Bender KG (2013) http://www.mubea.com (10.06.13)

Myers RH, Montgomery DC (1995) Response surface methodology: process and product optimization using designed experiments. Wiley & Sons, New York

Pan F, Zhu P (2011) Lightweight design of vehicle front end structure: contributions of multiple surrogates. Int J Veh Des 57(2–3):124–147

Pan F, Zhu P, Zhang Y (2010) Metamodel-based lightweight design of B-pillar with TWB structure via support vector regression. Comput Struct 88(1–2):36–44

Park JS (1994) Optimal Latin-hypercube designs for computer experiments. J Stat Plan Infer 39(1):95–111

Poli R, Kennedy J, Blackwell T (2007) Particle swarm optimization. Swarm Intell 1(1):33–57

Ryabkov N, Jackel F, Van Putten K, Hirt G (2008) Production of blanks with thickness transitions in longitudinal and lateral direction through 3D-strip profile rolling. Int J Mater Form Suppl 1(1):391–394

Sacks J, Welch WJ, Mitchell TJ, Wynn HP (1989) Design and analysis of computer experiments. Stat Sci 4(4):409–435

Schölkopf B, Smola AJ (2002) Learning with Kernels: support vector machines, regularization, optimization, and beyond. MIT Press, Cambridge

Schölkopf B, Smola AJ, Williamson RC, Bartlett PL (2002) New support vector algorithms. Neural Comput 12(5):1207–1245

Shi YL, Zhu P, Shen LB, Lin ZQ (2007) Lightweight design of automotive front side rails with TWB concept. Thin-Walled Struct 45(7):8–14

Singh A (2009) An artificial bee colony algorithm for the leaf-constrained minimum spanning tree problem. Appl Soft Comput 9(2):625–631

Song XG, Sun GY, Li GY, Zhao W, Li Q (2013) Crashworthiness optimization of foam-filled tapered thin-walled structure using multiple surrogate models. Struct Multidiscip Optim 47(2):221–231

Srinivasan D, Seow TH (2003) Evolutionary computation, CEC'03, 8–12 Dec. 4, Canberra, Australia, pp 2292–2297

Storn R, Price K (1997) Differential evolution-a simple and efficient heuristic for global optimization over continuous spaces. J Glob Optim 11(4):341–359

Sun GY, Li GY, Li Q (2012) Variable fidelity design based surrogate and artificial bee colony algorithm for sheet metal forming process. Finite Elem Anal Des 59:76–90

Sun GY, Xu FX, Li GY, Li Q (2014) Crashing analysis and multiobjective optimization for thin-walled structures with functionally graded thickness. Int J Impact Eng 64:62–67

Sun GY, Tian XY, Fang JG, Xu FX, Li GY, Huang XD (2015) Dynamical bending analysis and optimization design for functionally graded thickness (FGT) tube. Int J Impact Eng 78:128–137

Vapnik V (1995) The nature of statistical learning theory. Springer, Berlin

Vapnik V (1998) Statistical learning theory. Wiley, New York

Varma S, Simon R (2006) Bias in error estimation when using cross-validation for model selection. BMC Bioinf 791

Viana FAC, Haftka RT, Steffen V (2009) Multiple surrogates: how cross-validation errors can help us to obtain the best predictor. Struct Multidiscip Optim 39:439–457

Wu SR, Zhang XT, Lenk P (2001) Step function-a measure for frontal crash pulse and its applications. Int J Veh Des 26(4):385–394

Xiao Z, Fang JG, Sun GY, Li Q (2015) Crashworthiness design for functionally graded foam-filled bumper beam. Adv Eng Softw 85:81–95

Zhang Y, Lai XM, Zhu P, Wang WR (2006) Lightweight design of automobile component using high strength steel based on dent resistance. Mater Des 27(1):64–68

Zhang Y, Zhu P, Chen GL (2007) Lightweight design of automotive front side rail based on robust optimization. Thin-Walled Struct 45(7–8):670–676

Zhang HW, Liu LZ, Hu P, Liu XH (2012a) Numerical simulation and experimental investigation of springback in U-channel forming of tailor rolled blank. Int J Iron Steel Res 19(9):8–12

Zhang HW, Liu LZ, Hu P, Liu XH (2012b) Springback characteristics in U-channel forming of tailor rolled blank. Acta Metall Sin English Lett 25(3):207–213

Zhu P, Zhang Y, Chen GL (2009) Metamodel-based lightweight design of automotive front body structure using robust optimization. Proc Inst Mech Eng D J Automob Eng 223(9):1133–1147